Broadband dielectric spectroscopy study of Li^+ ion motions in the fast ionic conductor $Li_{3x}La_{2/3-x}TiO_3$ (x = 0.09); comparison with ^7Li NMR results

2003 J. Phys.: Condens. Matter 15 7571

(http://iopscience.iop.org/0953-8984/15/44/010)

INSTITUTE OF PHYSICS PUBLISHING JOURNAL OF PHYSICS: CONDENSED MATTER

J. Phys.: Condens. Matter **15** (2003) 7571–7584 PII: S0953-8984(03)65454-8

Broadband dielectric spectroscopy study of Li^+ ion motions in the fast ionic conductor $Li_{3x}La_{2/3-x}TiO_3$ ($x = 0.09$); comparison with ^7Li NMR results

O Bohnké[1,4], J C Badot[2] and J Emery[3]

[1] Laboratoire des Fluorures (UMR 6010 CNRS), Université du Maine, Avenue O Messiaen, 72085 Le Mans Cedex 9, France
[2] Laboratoire de Chimie Appliquée de l'Etat Solide (UMR 7574 CNRS), ENSCP, 11 rue P et M Curie, 75231 Paris Cedex 05, France
[3] Laboratoire de Physique de l'Etat Condensé (UMR 6087 CNRS), Université du Maine, Avenue O Messiaen, 72085 Le Mans Cedex 9, France

E-mail: odile.bohnke@univ-lemans.fr

Received 30 June 2003
Published 24 October 2003
Online at stacks.iop.org/JPhysCM/15/7571

Abstract

Microscopic motions of Li^+ ions in the fast ionic conductor $Li_{3x}La_{2/3-x}TiO_3$ ($x = 0.09$) are studied by dielectric spectroscopy in the frequency range from 10^3 to 4×10^9 Hz and in the temperature range from 200 to 400 K. Several dielectric relaxations are evidenced by this technique and can be ascribed to different motions of the Li^+ ions in the oxide. These motions are related to the Li^+ motions observed by means of ^7Li NMR and dc conductivity and already reported in previous papers. From these two complementary techniques, three motions of Li^+ ions are evidenced in the perovskite structure ABO_3: a slow motion that corresponds to the hopping of the Li^+ ions from one A-cage to the next vacant one through bottlenecks made of four oxygen ions and two fast motions that correspond to local motions of the mobile ions between their off-centred positions in the A-cage of the perovskite structure. A change in the mechanism of conduction is observed around 200 K. This change is attributed to a change in the dimensionality of the Li^+ ion motion from 2D to 3D as temperature is increased. At low temperatures ($T < 200$ K) both the local and the long range Li^+ ion motions happen in the (a, b) planes of the crystallographic structure (2D motion). As temperature increases, Li^+ ions experience the entire volume of the A-cage finally moving in three directions above 400 K (3D motion). This change is corroborated by the ratio of the activation energies in the two domains, i.e. 1.5, observed in T_1 versus $10^3/T$ plots as well as in the dc conductivity plot and in the dielectric relaxations versus $10^3/T$ plot. These results confirm the fact that, in $Li_{3x}La_{2/3-x}TiO_3$, the long range motion of Li^+ ions is evidenced by $T_{1\rho}$ and σ_{dc} and their local

[4] Author to whom any correspondence should be addressed.

motions in the A-site of the perovskite structure are evidenced by T_1 and by dielectric spectroscopy at frequencies higher than 1 MHz, in the temperature range investigated. Therefore, $T_{1\rho}$ and σ_{dc} can be compared since they are related to the same ionic motion. Finally, we found that the constant loss behaviour, observed by previous authors, is in fact the contribution of two quasi-Debye dielectric relaxations.

1. Introduction

The perovskite-type Li ion conductors $Li_{3x}La_{2/3-x}TiO_3$ have attracted much attention because of their high purely ionic conductivity, i.e., $\sigma = 10^{-3}$ S cm^{-1} for $x = 0.11$ at room temperature, first reported by Belous *et al* [1] and afterwards by Inaguma *et al* [2]. These compounds (hereafter called LLTO) belong to a solid solution group. The stability range of this solid solution is $0.06 < x < 0.14$ for compounds prepared below 1200 °C [3, 4]. Recently, Ibarra *et al* [5] have shown that this range could be extended by increasing the synthesis temperature to 1350 °C. Various unit cells, all derived from the perovskite, were proposed by different authors. A discussion of the above-proposed structural models appears in a previous paper [6]. However, most of these authors agree on the fact that LLTO consists of a doubled perovskite unit cell with $a = b \cong 3.87$ Å and $c \cong 2a$. Apart from the probable existence of a larger cell, due to a very slight tilting of the TiO_6 octahedra, it seems that the tetragonal unit cell ($a = a_p$ and $c \cong 2a_p$, space group $= P4/mmm$) can be used to approach the true structure. Indeed, this model is able to take into account both the superstructure lines and their evolution with the composition parameter x of the solid solution. Moreover, their intensities can be calculated well from the La^{3+} populations in the two different A-sites (1a and 1b sites) [4]. For these reasons we will use this model for the discussion in this paper. Local ordering inside this crystalline structure can arise locally via the non-uniform distribution of La^{3+} ions and vacancies among the A-sites (1a and 1b sites) of the ABO_3 perovskite lattice. 1a sites (named La1) are preferentially occupied by lanthanum and 1b sites (named La2) by vacancies (figure 1(a)), although neither has full occupancy [4]. This non-uniform distribution of La^{3+} ions leads to a La-rich layer (or La1 layer) and a La-poor layer (or La2 layer) giving rise to two A-cages with different sizes (figures 1(b) and (c)). A second type of partial order occurs through the breaking of the alternating stacking sequence of La1 and La2 layers along the c direction, as pointed out by Fourquet *et al* [4].

Li^+ ion mobility is affected by its environment and by the distribution of lanthanum and vacancies in the surrounding perovskite A-cages. Therefore, different environments around the A-sites may produce a distribution of activation energies of the ionic motion. This assumption, based on dc conductivity measurements and ^{7}Li NMR experiments, has been made and discussed by Bohnké *et al* [7]. However, these authors have shown that the particular feature displayed by the ^{7}Li NMR experimental curve around 200 K cannot be completely explained by the above-proposed model. Therefore, further studies have been carried out by means of ^{7}Li NMR (determination of T_1, $T_{1\rho}$ and T_2 relaxation times) and by impedance spectroscopy. They are reported in [8, 9] and [10] respectively. In all these experiments several motions of the Li^+ ion have been detected. However, the frequency window available in impedance spectroscopy (i.e. 1–10^7 Hz) does not entirely match the frequencies used in ^{7}Li NMR studies (i.e. 62.5 kHz for $T_{1\rho}$ and 116 MHz for T_1) and our results were thus partial. To complete these previous studies, we report in this paper a detailed study of the dielectric spectroscopy of LLTO in the broad frequency range from 10^3 to 4×10^9 Hz and in the temperature range from 200 to 400 K. This work affords further details on the local motion of Li^+ ions in this

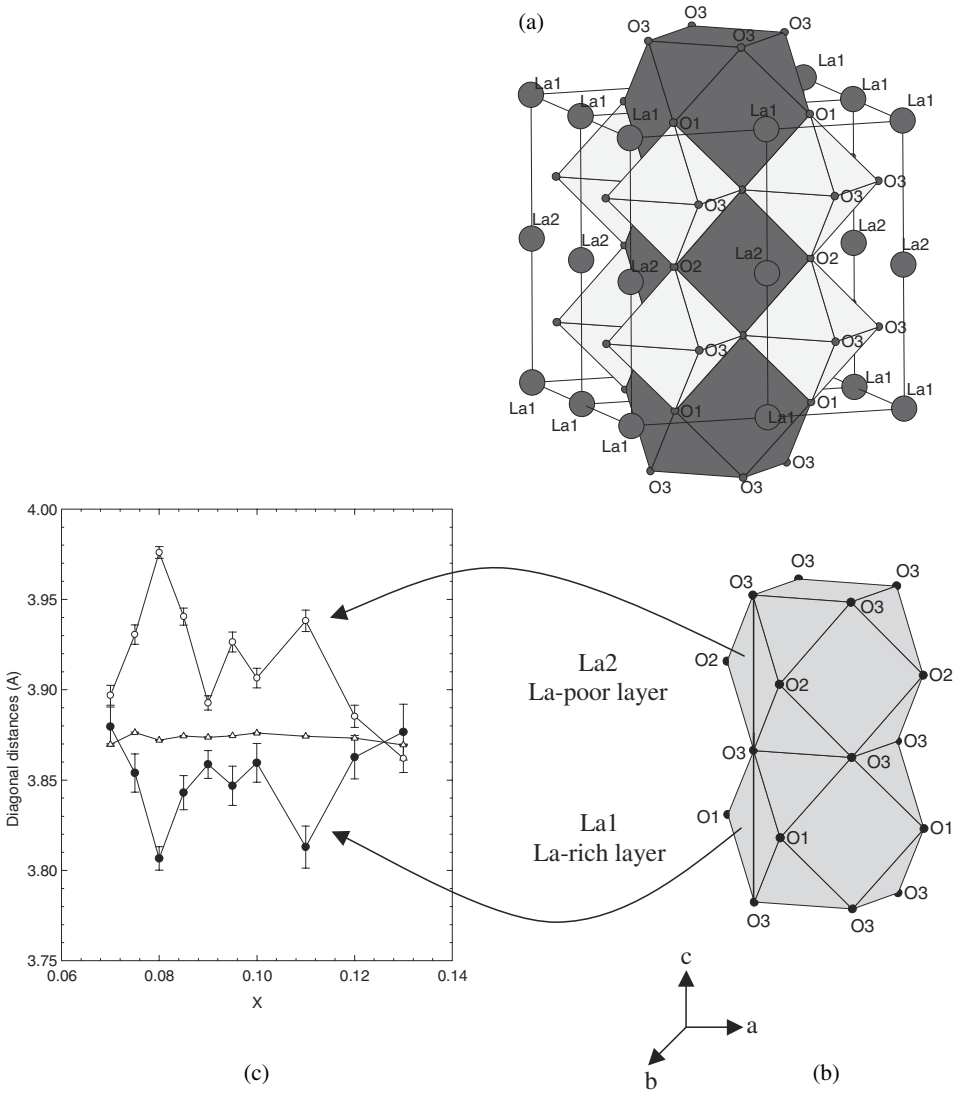

Figure 1. (a) A schematic view of the unit cell, at room temperature, based on the structural model in the space group $P4/mmm$. (b) A schematic view of the two A-cages La1 and La2 of the unit cell. (c) Bottleneck diagonals: ○ = O3–O3 in the *c* direction of the La2 layer, ● = O3–O3 in the *c* direction of the La1 layer, △ = O2–O2 = O1–O1 = O3–O3 in the *a* and *b* directions.

oxide and it enables us to describe the different motions that Li^+ undergoes in this material as a function of the temperature. A microscopic model for the dynamic behaviour of the mobile Li^+ ions is then proposed and discussed in accordance with the experimental data obtained by these different and complementary techniques.

2. Experimental details

2.1. Preparation of the solid solution compound

The solid solution compound, with composition $x = 0.09$, was prepared by conventional solid state reactions from stoichiometric amounts of TiO_2 (99.5%) from Riedel Haen, Li_2CO_3

(99.997%) from Aldrich and freshly dehydrated La_2O_3 (99.999%) from Rhone-Poulenc. The starting materials were mixed and pressed into pellets (diameter 13 mm, thickness ≈2 mm, $P = 0.25$ GPa). They were first heated at 850 °C for 4 h in a Pt crucible and then heated up to 1050 °C for 12 h. After grinding and pressing, the pellets were heated twice for 12 h at 1100 and 1150 °C respectively. After a new grinding, a last heating treatment was performed on small pellets (diameter 3 mm, thickness slightly smaller than 1 mm, $P = 4$ GPa) at 1250 °C for 12 h. The heating sweep rate was 5 °C min^{-1}. A natural cooling in the furnace followed all the heating treatments.

2.2. Dielectric spectroscopy

Permittivity and conductivity measurements were performed in a broad frequency range from 10^3 to 4×10^9 Hz, using an impedance analyser (HP 4291) and simultaneously two network analysers (HP 8510B and HP 8751A). Experiments were carried out in the 200–400 K temperature range. The experimental device consists of a coaxial cell (APC7 standard) in which the cylinder-shaped sample fills a discontinuity between the inner conductor and a short circuit [11–15]. The sample, whose thickness ℓ is around 1 mm, has the same radius ($r = 1.5$ mm) as the inner conductor and has front faces covered with a silver layer to ensure good electrical contact. Knowledge of the sample complex admittance Y^*, computed from measurements of the complex reflection coefficient, allows one to determine the complex permittivity $\varepsilon^*(\omega)$ according to

$$Y^* = (G + \mathrm{i}C\omega) = \mathrm{i}\frac{2\pi\gamma r}{\omega\mu_0\ell}\frac{J_1(\gamma r)}{J_0(\gamma r)} \tag{1}$$

where G and C are the conductance and the capacitance of the sample respectively, $\omega = 2\pi\nu$ the angular frequency, $\mathrm{i} = (-1)^{1/2}$, $\gamma = \gamma_0(\varepsilon^*(\omega))^{1/2}$ with $\gamma_0 = \omega/c$ ($c = 3 \times 10^8$ m s^{-1}). μ_0 is the free space permeability. ℓ and r are the thickness and the radius of the sample respectively. J_0 and J_1 are zero- and first-order Bessel functions of the first kind, respectively. The expression (1) is valid only for a thickness of the sample lower than the half-wavelength. To calculate the complex permittivity $\varepsilon^*(\omega) = \varepsilon'(\omega) - \mathrm{i}\varepsilon''(\omega)$, we used an iterative method derived from the gradient method [16]. We recall that knowledge of the complex permittivity $\varepsilon^*(\omega)$ permits the calculation of the complex conductivity $\sigma^*(\omega) = \mathrm{i}\omega\varepsilon_0\varepsilon^*(\omega)$ and also the complex resistivity $\rho^*(\omega) = [\sigma^*(\omega)]^{-1}$. Dielectric and conductivity spectra were constructed from about 400 measurements with an accuracy of from 3 to 5%.

2.3. ^{7}Li NMR investigation

T_1 and $T_{1\rho}$ relaxation time measurements were carried out in the 150–900 K temperature range. The Larmor frequency for ^{7}Li was $\nu_0 = 116$ MHz. The amplitude of the radio-frequency field was $\nu_1 = 62.5$ kHz. The experimental set-ups and the procedure used to determine the longitudinal relaxation times, T_1, and the longitudinal relaxation times in the rotating frame, $T_{1\rho}$, were described in [7–9].

3. Results

Figure 2(a) shows the frequency dependence of the real part of the conductivity, σ' (hereafter called σ), at different temperatures and in the frequency range from 10^3 to 4×10^9 Hz, for the $x = 0.09$ solid solution compound. The grain boundaries are responsible for the strong decrease of the real part of the conductivity between 10^3 and 10^5 Hz. The contribution of the electrode/electrolyte interface to σ appears at lower frequencies [10] and is not observable in

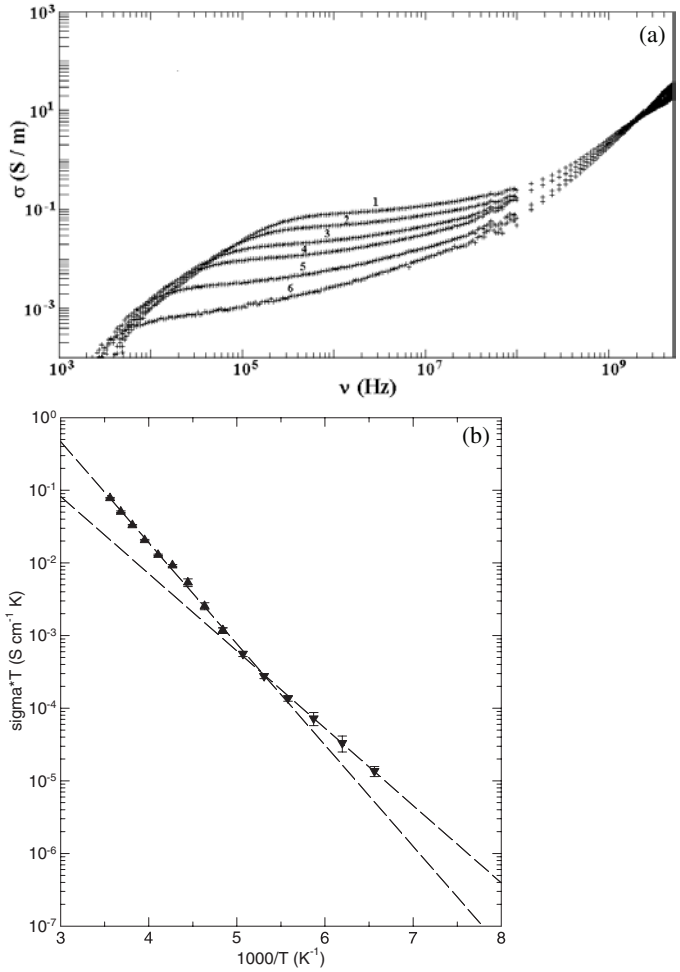

Figure 2. (a) The real part of the conductivity σ as a function of frequency ν for $Li_{3x}La_{2/3-x}TiO_3$ ($x = 0.09$) at (1) 300 K, (2) 285 K, (3) 268 K, (4) 256 K, (5) 248 K and (6) 230 K. (b) The dc conductivity as a function of the inverse of temperature (T^{-1}) for $Li_{3x}La_{2/3-x}TiO_3$ ($x = 0.09$).

this frequency range. For frequencies between 10^5 and 10^7 Hz at room temperature (curve 1), the long range conductivity process through the sample is indicated by the presence of a plateau corresponding to the dc conductivity of the Li^+ ion in the oxide. The dc conductivity is thermally activated and decreases as temperature decreases (curves 1–6). At high frequency ($\nu > 10^8$ Hz) the conductivity displays a dispersive behaviour, as generally observed in ionic conductors. These results are in perfect accordance with the results obtained by impedance spectroscopy, in a smaller frequency range, reported in [10] for $x = 0.10$. Figure 2(b) presents the bulk dc conductivity of this compound in the 150–300 K temperature range. It reveals a change of conduction mechanism around 200 K, as previously observed and discussed in [10]. The dc conductivity, σ_{dc}, follows the classical Arrhenius law:

$$\sigma_{dc}T = \sigma_0 \exp(-E_a/RT). \tag{2}$$

Below 200 K, the activation energy is 0.21 eV and the pre-exponential factor $\sigma_0 = 1.28 \times 10^2$ S cm^{-1} K. Above 200 K, the activation energy increases to 0.28 eV and the pre-exponential

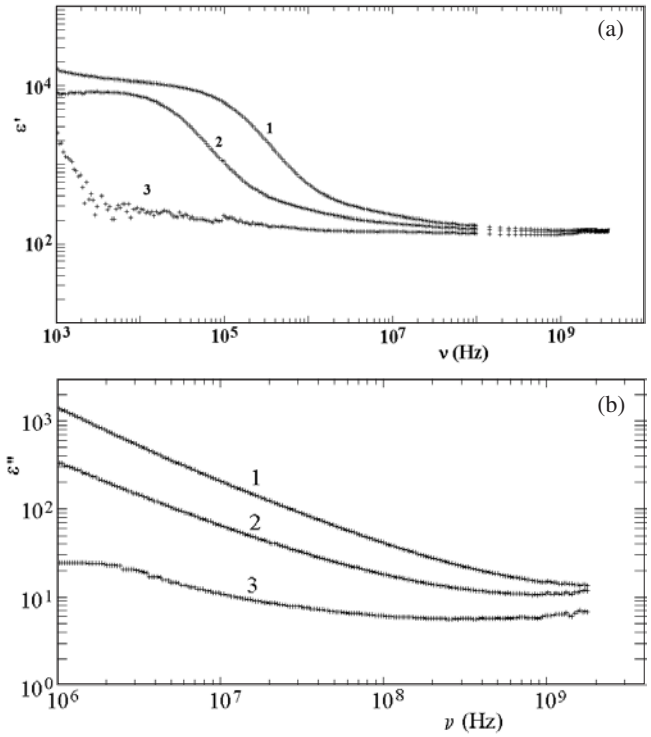

Figure 3. (a) The real part (ε') of the permittivity as a function of frequency ν for $Li_{3x}La_{2/3-x}TiO_3$ ($x = 0.09$) at (1) 300 K, (2) 256 K and (3) 200 K. (b) The imaginary part (ε'') of the permittivity as a function of frequency ν for $Li_{3x}La_{2/3-x}TiO_3$ ($x = 0.09$) at (1) 300 K, (2) 256 K and (3) 200 K.

factor increases to 7.06×10^3 S cm^{-1} K. The σ_0 increase suggests that the number of long range moving ions increases as temperature increases; some Li^+ ions may be trapped in the A-cage of the structure at low temperature.

Figure 3 shows the frequency dependence of the permittivity for the $x = 0.09$ solid solution compound, from 200 (curve 3) to 300 K (curve 1). Figure 3(a) presents the real part of the permittivity, ε', and figure 3(b) the imaginary part, ε''. The ε' plot, at 300 K (curve 1), evidences the polarization of two different interfaces: the grain boundary interfaces responsible for the increase of ε' around 10^6 Hz and the quasi-blocking electrode/electrolyte interface responsible for the increase of ε' at frequencies below 10^3 Hz. As temperature decreases, these frequencies decrease and these two interfaces almost disappear from the plots, as shown at 200 K (curve 3). Figure 3(b) shows the dielectric loss, ε'', as a function of frequency. This figure seems to show the existence of a constant or nearly constant (dielectric) loss regime at high frequency. This behaviour is particularly well observed for the lower temperature ($T = 200$ K), as shown by curve 3. This behaviour has been previously reported in the $Li_{0.18}La_{0.61}TiO_3$ compound by Leon *et al* [17, 18]. This result will be discussed later in this paper.

Figure 4(a) presents the experimental data of the permittivity obtained at 300 K. For dielectric spectroscopy, the main problem lies in the decomposition of the dielectric spectra into different relaxations. Since not all the dielectric relaxations are clearly observed in the Bode representation, it is more suitable to use Cole–Cole (CC) plots, i.e. $\varepsilon'' = f(\varepsilon')$ as shown in figure 4. It is possible to evidence dielectric relaxations due to interfacial polarization (e.g. grain boundaries) and to dipolar reorientation below the phonon frequencies in ionic

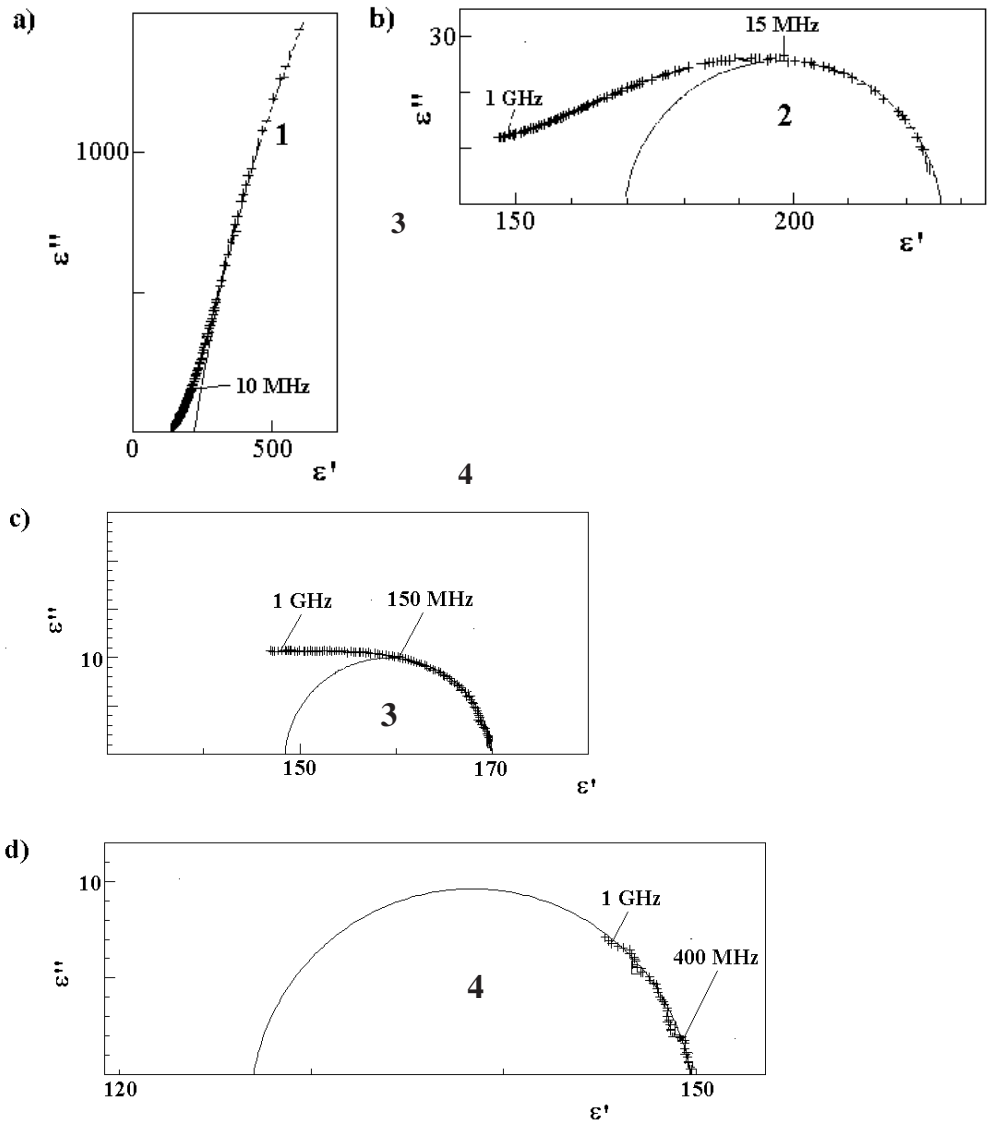

Figure 4. (a) A CC plot of the imaginary part $\varepsilon''(\omega)$ versus the real part $\varepsilon'(\omega)$ of the permittivity $\varepsilon^*(\omega)$ at 300 K for $Li_{3x}La_{2/3-x}TiO_3$ ($x = 0.09$); (b) the second relaxation domain (forward–backward hopping) obtained after subtracting the first relaxation domain (grain boundary polarization); (c) the third relaxation domain (local motion) obtained after subtracting the second relaxation domain; (d) the fourth relaxation domain (fast local motion) obtained after subtracting the third relaxation domain.

conductive ceramics. The dipolar reorientation is generally due to localized motions of the ions. All these phenomena occur at different characteristic frequencies and can then be separated by a decomposition procedure applied to the CC plots. When the frequency increases, the relaxations appear in the following order: (1) relaxation due to the polarization of the grain boundaries and (2) dipolar relaxations (ion hopping). The more localized the ionic hopping, the higher the frequency of this dipolar relaxation. The dielectric relaxations are generally

described by the Havriliak–Negami (HN) function of the complex permittivity [19], written as follows:

$$\varepsilon^*(\omega) = \varepsilon_{\mathrm{HF}} + \frac{\varepsilon_{\mathrm{LF}} - \varepsilon_{\mathrm{HF}}}{(1 + (\mathrm{i}\omega\tau)^{1-\alpha})^{\beta}} \tag{3}$$

where $\varepsilon_{\mathrm{LF}}$ and $\varepsilon_{\mathrm{HF}}$ are respectively the low and high frequency limits of the permittivity. τ is an evaluation of the characteristic timescale of the interface polarization and dipolar reorientation. The corresponding relaxation frequency is $\nu_{\mathrm{r}} = (2\pi\tau)^{-1}$. The parameters α and β range between 0 and 1 and determine the degree of deviation from the ideal Debye function for which $\alpha = 0$ and $\beta = 1$. Dielectric relaxations due to the grain boundary polarization or to local charge hopping [15] are often fitted by the CC function [20, 21] for which $\beta = 1$.

The low frequency region, domain 1 ($\nu < 10^6$ Hz), is described by a circular arc and corresponds to a quasi-Debye relaxation due to the grain boundary polarization. This relaxation is also shown in figure 3(a) (curve 1) as a sigmoidal-shaped curve with a strength of relaxation $\Delta\varepsilon = (\varepsilon_{\mathrm{LF}} - \varepsilon_{\mathrm{HF}}) \approx 9800$.

After subtracting relaxation domain 1, figure 4(b) is obtained. Domain 2, which then appears, corresponds to a dielectric relaxation described by the CC function with a parameter $\alpha \approx 0.07$, a strength of relaxation $\Delta\varepsilon \approx 55$ and a relaxation frequency $\nu_{\mathrm{r2}} \approx 1.5 \times 10^7$ Hz (or a relaxation time $\tau_2 \approx 10^{-8}$ s) at 300 K.

After subtracting this second contribution to the experimental data, figure 4(c) is obtained. This plot evidences the presence of a nearly constant loss which is clearly observed above 2×10^8 Hz. The low frequency part of this plot is well fitted by a circular arc (domain 3) corresponding to a quasi-Debye relaxation ($\alpha \approx 0.04$) with a relaxation frequency $\nu_{\mathrm{r3}} \approx 1.5 \times 10^8$ Hz (or a relaxation time $\tau_3 \approx 10^{-9}$ s) at 300 K and $\Delta\varepsilon \approx 22$. Finally, figure 4(d) is obtained after subtracting this third relaxation from the experimental data. A new circular arc (domain 4) is well fitted by a circular arc corresponding to a quasi-Debye relaxation ($\alpha \approx 0.07$) with a relaxation frequency $\nu_{\mathrm{r4}} \approx 3 \times 10^9$ Hz (or a relaxation time $\tau_4 \approx 5.3 \times 10^{-11}$ s) at 300 K and $\Delta\varepsilon \approx 22$. This result clearly shows that the constant loss shown in figure 3(b) is an apparent constant loss and is in fact the result of the presence of the two relaxation processes described by domains 3 and 4. The three relaxations 2, 3 and 4, which have been evidenced, are thus due to three dipolar motions of ions.

Figure 5 shows that the temperature dependence of the three relaxation frequencies ν_{r2}, ν_{r3} and ν_{r4} follows an Arrhenius law below room temperature,

$$\nu_{\mathrm{r}i} = \nu_{\mathrm{a}i} \exp\left(-\frac{E_i^{\mathrm{dm}}}{kT}\right) \tag{4}$$

where $i = 2$, 3 or 4. E_i^{dm} and $\nu_{\mathrm{a}i}$ are respectively the activation energy and the attempt frequency of these dipolar motions. Table 1 summarizes the results obtained for the three relaxations. They are characterized by the same mean attempt frequency which lies in the range of the LO phonon frequency (10^{12}–10^{13} Hz). They are then associated with the same type of charge carrier, i.e. Li^+ ions. These relaxations can then be associated to three different motions of the Li^+ ions in the structure with different activation energies in the temperature range from 200 to 300 K. Since the activation energy of relaxation 2 is the same as the dc conductivity one, it describes a motion corresponding to a forward–backward hopping from cage to cage. Relaxations 3 and 4 are thus due to lithium motions confined in the cages. We should note that the ratio of the activation energies of the relaxations 3 and 4 is $E_3^{\mathrm{dm}}/E_4^{\mathrm{dm}} = 3/2$.

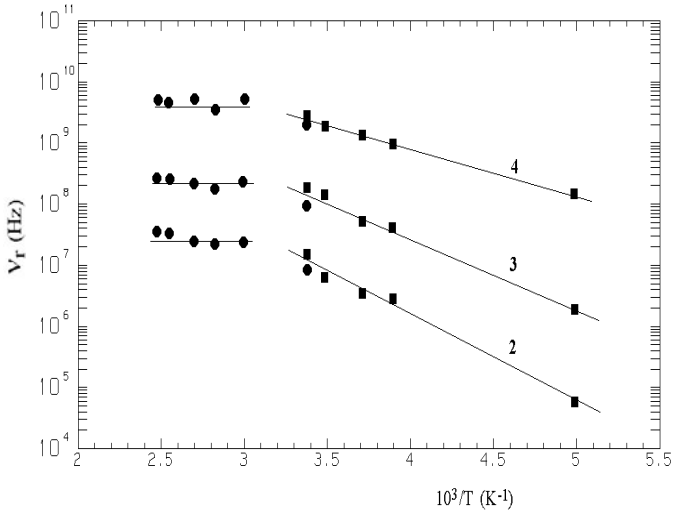

Figure 5. The relaxation frequency ν_r as a function of the inverse of temperature (T^{-1}) for forward–backward hopping of Li^+ ions *(domain 2)* and Li^+ local motions *(domains 3 and 4)*.

Table 1. The activation energy E_a (eV), attempt frequency ν_a (Hz) and correlation time τ_c (s) at 300 K obtained by the different techniques. Results in bold type are from [9].

	E_a (eV)	ν_a (Hz)	τ_c (s) at 300 K
Dielectric relaxations			
2 (1.5×10^7 Hz)	0.29	5.5×10^{12}	10^{-8}
3 (1.5×10^8 Hz)	0.23	7.1×10^{12}	10^{-9}
4 (3×10^9 Hz)	0.15	6.3×10^{12}	5.3×10^{-11}
^{7}Li NMR			
$T_{1\rho}$	**0.20**	1.6×10^9	1.5×10^{-6}
T_1 (HT)	**0.20**	4.5×10^{11}	5×10^{-9}
		7.1×10^{11} (BPP model)	
T_1 (BT)	**0.14**	3.0×10^{11}	8×10^{-10}
dc conductivity			
200 K $< T <$ 300 K	0.28		10^{-6}
$T <$ 200 K	0.21		

4. Discussion

In previous papers, we discussed the ^{7}Li NMR results that we obtained on LLTO [8, 9, 22]. We can summarize the results obtained as follows:

(i) two types of Li^+ ion with slightly differing environments are present in LLTO (it is worth noting that no experimental evidence exists, at the time of our study, of the location of one kind of Li^+ ion in a particular layer, La1 or La2, of the structure);
(ii) T_1 and $T_{1\rho}$ relaxation times measurements show that these ions undergo two types of motion: a fast one probed at high frequency (116 MHz) by means of the longitudinal relaxation time T_1 (as shown in figure 6 and [9]) and a slow one probed at lower frequency (62.5 kHz) by means of the longitudinal relaxation time in the rotating frame $T_{1\rho}$ (as shown in figure 7 and [9]);

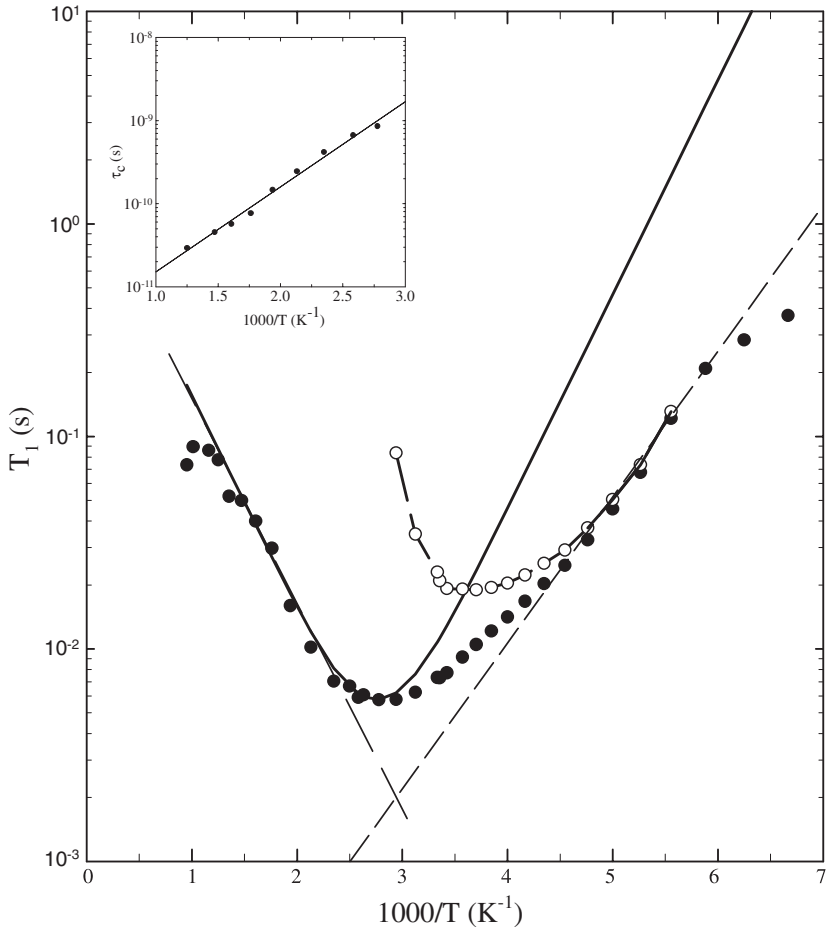

Figure 6. A logarithmic plot of the longitudinal relaxation time T_1 for ^{7}Li ($\nu_0 = 116$ MHz) as a function of the inverse of temperature for LLTO ($x = 0.11$). The dashed lines represent the linear regressions of the data at low ($E_a = 0.14$ eV) and high temperatures ($E_a = 0.20$ eV). The full curves represent the calculated T_1 obtained from BPP model. The inset curve shows the variation of the correlation time τ_c as a function of the inverse of temperature.

(iii) the two types of Li^+ ion can be differentiated by their slow motion (two $T_{1\rho}$ and two T_2) but not by their fast motion (only one T_1 is observed);
(iv) finally, all these NMR relaxation time curves and the dc conductivity curve (figure 2(b)) display a particular behaviour around 200 K.

From the minima of the T_1 and $T_{1\rho}$ curves, it can be found that the correlation time of the fast motion is 1.4×10^{-9} s at 350 K and the correlation time of the slow motion is 2.5×10^{-6} s at 280 K (at the minimum, $\omega_0\tau_c \approx 1$ for T_1 and $\omega_1\tau_c \approx 1$ for $T_{1\rho}$).

In the previous study [9] we determined, from the slopes of the high and low temperature parts of T_1 and from the slope of the high temperature part of $T_{1\rho}$, the activation energies of the different motions of the Li^+ ions. Furthermore, since it is postulated that the correlation times are thermally activated and follow the Arrhenius law, we can determine the correlation times at 300 K and the corresponding attempt frequency, ν_a, of these motions. Table 1 summarizes these results. The bold values correspond to results that already appeared in [9].

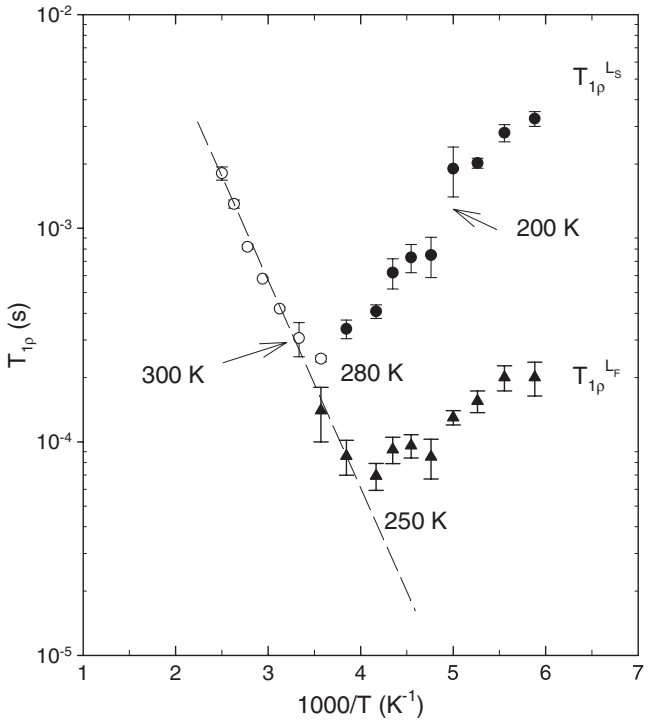

Figure 7. A logarithmic plot of the longitudinal relaxation times in the rotating frame $T_{1\rho}$ for ^{7}Li ($\nu_1 = 62.5$ kHz) as a function of the inverse of temperature for LLTO ($x = 0.11$). The dashed line represents the linear regression of the data at high temperatures ($E_a = 0.20$ eV).

In order to go further in the analysis of the NMR data, we determined herein the correlation time, τ_c, as a function of temperature, in the temperature range from 360 to 800 K, by using the Bloembergen–Purcell–Pound (BPP) model [23]. This model assumes an isotropic motion of particles (or a 3D motion) and a pure exponential correlation function. According to this model, T_1 follows the relationship

$$\frac{1}{T_1} = C\left(\frac{\tau_c}{1+(\omega_0\tau_c)^2} + \frac{4\tau_c}{1+(2\omega_0\tau_c)^2}\right) \tag{5}$$

with $\omega_0 = 2\pi\nu_0$ (ν_0 is the Larmor frequency for ^{7}Li). The value of C (i.e., $C = 8.9\times10^{10}\ s^{-2}$) is determined from the minimum of the T_1 versus $1000/T$ curve, where $\omega_0\tau_c \approx 1$ (figure 6). The plot of τ_c versus $1000/T$ is shown in the inset of figure 6. The correlation time is thermally activated and follows an Arrhenius law: the activation energy of this motion is found to be 0.20 eV. This activation energy is very close to the result obtained previously for this range of temperature (see [9] and table 1). This validates the use of the BPP model in the high temperature regime, confirming the assumption of a 3D motion of the Li^+ ion in this temperature range. The attempt frequency, calculated from the Arrhenius law, is found to be $\nu_a = 7.1\times10^{11}$ Hz.

Figure 6 clearly reveals that a change of mechanism occurs between 360 and 200 K. Below 360 K, the theoretical BPP curve does not account for the experimental data, confirming that a 3D motion is no longer valid. A new mechanism of Li^+ motion can then be invoked. On subtracting the BPP curve obtained at high temperature from the experimental data, the resulting curve (the dashed curve in figure 6) shows a minimum at 270 K. This curve represents

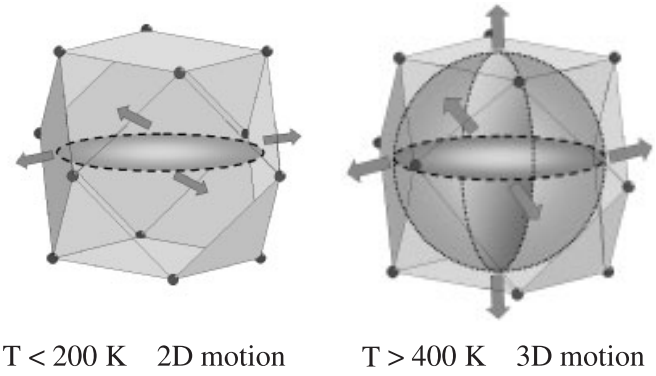

Figure 8. A schematic representation of the dimensionality change of the Li^+ motion in LLTO from 2D below 200 K to 3D above 400 K.

a second motion of the Li^+ ion in the oxide with a correlation time determined at this minimum, i.e., 1.4×10^{-9} s at 270 K, and an activation energy of 0.14 eV. This second motion of the Li^+ ion is faster and requires a lower activation energy than the previous one. Table 1 summarizes all these results (the correlation times of the different motions were calculated at 300 K, according to the Arrhenius law and to the activation energy found previously). This table enables us to compare the different motions observed by means of dc conductivity, dielectric spectroscopy and ^{7}Li NMR.

The most important point evidenced by these techniques is the presence of different motions of the Li^+ ions in LLTO. The slow motion is probed by means of ^{7}Li NMR through the spin–lattice relaxation times in the rotating frame $T_{1\rho}$, by means of dielectric spectroscopy at frequencies of the order of 10 MHz (relaxation 2 in figure 4) and by means of σ_{dc}. As suggested in previous papers [8–10], this motion can be attributed to Li^+ motion from A-cage to A-cage leading to the dc conductivity. Between 200 and 300 K, the activation energy of the migration process increases to 0.28 eV. Two fast motions are probed by means of ^{7}Li NMR through the spin–lattice relaxation time T_1 and by dielectric spectroscopy. They correspond to localized motions of Li^+ ions inside the A-cage of the perovskite structure. A very fast one, dominant at low temperature ($T < 200$ K), corresponds to a two-dimensional motion of the moving ion. It occurs in the (a, b) planes of the structure. The other one, dominant at high temperature ($T > 400$ K), is slightly slower than the previous one. It corresponds to a three-dimensional motion of the Li^+ ion inside the A-cage. Figure 8 shows these motions in an A-cage schematically; at $T < 200$ K the disc represents the positions occupied by the Li^+ ion during its motion in the cage and for $T > 400$ K the sphere represents the volume occupied by this ion in the cage. The Li^+ motion in the (a, b) plane can be easier than that in the c direction because of the bigger size of the bottlenecks, as shown in figure 1(a). This can explain the low activation energy observed for the two-dimensional motion of the Li^+ ions. Between 200 and 300 K both motions are evidenced by means of ^{7}Li NMR (fractal dimension motion of the ions) and also by dielectric spectroscopy performed in this temperature range (relaxations 3 and 4).

However, for each motion the activation energy and the attempt frequency found by dielectric spectroscopy or impedance spectroscopy are always higher than the ones found by means of NMR. As previously discussed by Richards [24], this difference may result from the correlated hopping of many Li^+ ions. Indeed, the frequency measured through dielectric or impedance spectroscopy is a correlated frequency that describes the collective motion of all the mobile ions, whereas the frequency measured through NMR relaxation is related to the

motion of a single ion. The ratio of the activation energies found by the two techniques varies from 0.70 for the A-cage to A-cage motion of Li^+ to around 0.9 for the localized motions inside the A-cage. This suggests that the long range motion of Li^+ ions is much more correlated than the localized motion—that is, it is a more random one.

The change of dimensionality is undoubtedly shown by the ratio of 1.5 obtained between the activation energies of the two motions in dielectric spectroscopy, T_1 experiments and dc conductivity studies. This change of dimensionality explains completely the unusual behaviour, observed around 200 K, in ^{7}Li NMR, dc conductivity and ac conductivity parameters as shown in [10]. It is due to the vibration of the oxygen ions that increases as temperature increases and that opens bottlenecks and creates new pathways for the Li^+ ion to move along in the structure. This result is also in accordance with the presence of a distribution of activation energies previously suggested in one of our early papers on this topic [7]. Finally, we should note that the almost constant loss observed by Leon *et al* [17, 18] is not a constant loss phenomenon but is due to the presence of two relaxations in this frequency domain.

An incorrect relationship between the experimental parameters and the hopping process may also be invoked since it is not yet clear to what extent correlation can produce important differences. The interactions involved in the two techniques are different: in dielectric and dc conductivity studies we look at a vector parameter (polarization), whereas in NMR studies the interaction is represented by a tensor operator of rank 2 (dipolar or quadrupolar). In both experiments, the interactions fluctuate owing to the motion of Li^+ ions and of their environment. It is clear that these experiments probe the same ionic motion but through different fluctuations of the interactions. In ionic dynamics, the common feature is motion that is characterized by a correlation time. In both techniques it is possible to clearly identify the different motions of the mobile species as soon as the experimental frequency window corresponds. However, further studies are necessary to quantitatively explain the differences observed in correlation time, activation energy and attempt frequency of the ionic motions.

5. Conclusions

Dielectric and impedance spectroscopy along with ^{7}Li NMR relaxation time experiments allowed us to determine the microscopic motions of Li^+ ions in the perovskite structure of LLTO. It was possible to distinguish long range motion of the mobile ions from A-cage to A-cage that ensures dc conductivity and localized motions of these ions inside the A-cage. A change of dimensionality, from 2D to 3D, occurs when temperature increases above 200 K. This behaviour leads to an increase of the activation energy with a ratio of $\approx$1.5. This particular increase of the activation energy with a ratio of 1.5 is observed in dc conductivity, T_1 relaxation time and dielectric relaxations.

This work shows clearly that several techniques are necessary to reveal microscopic ionic motions in a material. These techniques are complementary and each can afford some of the information required to describe the ionic motion.

References

[1] Belous A G, Novitskaya G N, Polyanetskaya S V and Gornikov Y I 1987 *Russ. J. Inorg. Chem.* **32** 156
[2] Inaguma Y, Chen L, Itoh M, Nakamura T, Uchida T, Ikuta H and Wakihara M 1993 *Solid State Commun.* **86** 689
[3] Robertson A D, Garcia-Martin S, Coats A and West A R 1995 *J. Mater. Chem.* **5** 1405
[4] Fourquet J-L, Duroy H and Crosnier-Lopez M-P 1996 *J. Solid State Chem.* **127** 283
[5] Ibarra J, Varez A, Leon C, Santamaria J, Torres-Martinez L M and Sanz J 2000 *Solid State Ion.* **134** 219
[6] Bohnké O, Duroy H, Fourquet J-L, Ronchetti S and Mazza D 2002 *Solid State Ion.* **149** 217

[7] Bohnké O, Emery J, Veron A, Fourquet J-L, Buzaré J-Y, Florian P and Massiot D 1998 *Solid State Ion.* **109** 25
[8] Emery J, Bohnké O, Fourquet J-L, Buzaré J-Y, Florian P and Massiot D 2001 *C. R. Acad. Sci.* **4** 845
[9] Emery J, Bohnké O, Fourquet J-L, Buzaré J-Y, Florian P and Massiot D 2002 *J. Phys.: Condens. Matter* **14** 523–39
[10] Bohnké O, Emery J and Fourquet J-L 2003 *Solid State Ion.* **158** 119
[11] Getsinger W J 1966 *IEEE Trans. Microw. Theory Tech.* **14** 58
[12] Kolodziej H and Sobscyk L 1971 *Acta Phys. Pol.* A **39** 59
[13] Badot J-C, Fourrier-Lamer A and Baffier N 1985 *J. Physique* **46** 2107
[14] Pecquenard B, Badot J-C, Baffier N and Belhadj-Tahar N 1997 *Phys. Status Solidi* a **159** 469
[15] Badot J-C, Bianchi V, Baffier N and Belhadj-Tahar N 2002 *J. Phys.: Condens. Matter* **14** 6917
[16] Belhadj-Tahar N, Fourrier-Lamer A and De Chanterac H 1990 *IEEE Trans. Microw. Theory Tech.* **38** 1
[17] Leon C, Rivera A, Varez A, Sanz J, Santamaria J and Ngai K L 2001 *Phys. Rev. Lett.* **86** 1279
[18] Rivera A, Varez A, Sanz J, Santamaria J and Leon C 2001 *J. Alloys Compounds* **323/324** 545
[19] Havriliak S and Negami S 1967 *Polymer* **8** 161
[20] Cole R H and Cole K S 1941 *J. Chem. Phys.* **9** 341
[21] Jonscher A K, Pickup C and Zaidi S H 1986 *Semicond. Sci. Technol.* **1** 71
[22] Emery J, Buzaré J-Y, Bohnké O and Fourquet J-L 1997 *Solid State Ion.* **99** 41
[23] Bloembergen N, Purcell E M and Pound R V 1948 *Phys. Rev.* **73** 679
[24] Richards P M 1979 *Physics in Superionic Conductors* (*Springer Topics in Current Physics*) (Berlin: Springer) p 141